frontiers | Frontiers in Materials

TYPE Original Research
PUBLISHED 07 January 2025
DOI 10.3389/fmats.2024.1461271

OPEN ACCESS

EDITED BY
Oleksandr Menshykov,
University of Aberdeen, United Kingdom

REVIEWED BY
Antonio Pellegrino,
University of Bath, United Kingdom
Zhongnian Yang,
Qingdao University of Technology, China

*CORRESPONDENCE
Weiyu Li,
wylcumtb@163.com

RECEIVED 08 July 2024
ACCEPTED 17 December 2024
PUBLISHED 07 January 2025

CITATION
Li W, Fang S, Zhu Y and Li G (2025) Study on dynamic mechanical properties of frozen weakly cemented rock under lateral constraint.
Front. Mater. 11:1461271.
doi: 10.3389/fmats.2024.1461271

Study on dynamic mechanical properties of frozen weakly cemented rock under lateral constraint

Weiyu Li[1,2]*, Shizheng Fang[3], Ye Zhu[4] and Guangming Li[5]

[1]Joint National-Local Engineering Research Centre for Safe and Precise Coal Mining, Anhui University of Science and Technology, Huainan, China, [2]School of Safety Science and Engineering, Anhui University of Science and Technology, Huainan, China, [3]China Jingye Engineering Co., Ltd., Beijing, China, [4]School of Mining Engineering, Anhui University of Science and Technology, Huainan, China, [5]Shandong Succeed Mining Safety Engineering Co., Ltd., Taian, China

Weakly cemented red sandstone is common in the construction of shaft engineering in western China. Based on the actual working conditions, the dynamic mechanical behavior of this kind of rock under the combined action of multiple variables was studied. Based on the freezing temperature of the freezing method for shaft construction, the experimental temperature gradient was set at 25°C to −25°C. Using an modified split Hopkinson pressure bar (SHPB) experimental system, the dynamic mechanical response of frozen weak-cemented red sandstone under lateral constraints was studied. Taking dynamic and static stress fields and temperature fields as the entry point, the relationship between dynamic load, confining pressure, temperature, and dynamic mechanical characteristics parameters of weakly cemented rock is established, and the strain rate effect, lateral constraint effect, and negative temperature effect of dynamic compressive strength are analyzed. The research results show that: 1) The confining pressure changes synchronously with the axial dynamic load, and undergoes three stages: rapid increase, slow increase, and unloading rebound. 2) Under the combined effects of multiple variables, the dynamic mechanical behavior of the rock shows obvious compaction and rebound characteristics. 3) The dynamic compressive strength of the rock is jointly affected by strain rate, confining pressure, and temperature. Among them, lateral constraints have a strengthening effect. The dynamic compressive strength increases exponentially with increasing strain rate, and increases first and then decreases with decreasing temperature. At the same time, the degree of rock fragmentation is consistent with its strength characteristics. The research results have certain reference significance for the engineering design and safe operation and maintenance of frozen rock structures under dynamic loading.

KEYWORDS

SHPB, weakly cemented soft rock, negative temperature, lateral constraint, dynamic mechanical properties

1 Introduction

In the western region of China, there is a widespread distribution of soft rock strata from the Mesozoic Jurassic and Cretaceous, which are characterized by low

cementation. These rocks have poor cementation between particles, low strength, and are prone to disintegration and argillitization when exposed to water (Zhang et al., 2023; Chen S. et al., 2022; Li et al., 2022; Fang et al., 2023). When subjected to external dynamic loads, such as blasting vibrations, earthquakes, or vibrations from construction machinery, cracks can easily form in the rock mass, creating hydraulic pathways. This results in the rock mass being saturated with water, significantly reducing its strength and posing safety risks to engineering projects (Cai et al., 2019; Zheng et al., 2015; Wang and Yang, 2022; Xu et al., 2024). In engineering projects, artificial freezing methods are often used to pre-treat these types of rock masses (Fang et al., 2023; Bai et al., 2020; Liu et al., 2023; Shan et al., 2021), followed by excavation using dynamic methods. When the frozen rock mass is subjected to dynamic loading, the shaft wall and other structures provide lateral constraints on the rock strata. Under this condition, the occurrence environment of weakly cemented rocks is complex. Weak cementation and multi-field coupling states can affect the dynamic mechanical response of rocks, thereby affecting construction safety and the safe service of buildings and structures.

Many scholars have conducted extensive research on the dynamic characteristics of rocks under confined conditions. The main method is to use a metal sleeve to cover the rock sample to be loaded, and apply high-density lubricant inside the sleeve as a couplant to transmit pressure. The strain gauge attached to the outside of the metal sleeve is used to collect the circumferential deformation signal outside the sleeve (Bi et al., 2024), and then the elastic thick-walled cylinder theory is used to calculate the radial normal stress at any point inside the sleeve (Luo et al., 2011; Luo et al., 2014; Bragov et al., 2008). The passive confining pressure is applied using two methods: a thin-walled sleeve and a thick-walled sleeve. The similarities between the two methods are that the inner diameter of the sleeve and the specimen diameter require high precision and close fit, incident waves are used as triggering signals, and strain signals are collected by strain gauges attached to the axial direction of the incident and transmission bars and the circumferential direction of the outer wall of the sleeve. The difference lies in that the theory of the thick-walled sleeve is based on the premise that the sleeve always deforms elastically, while the theory of the thin-walled sleeve takes into account the plastic properties of the sleeve material. The thin-walled sleeve method is mainly suitable for testing metal materials, while the thick-walled sleeve method is more suitable for testing rock materials. Research on the dynamic mechanical properties of different types of rocks and rock-like materials under passive confining pressure conditions has found that the existence of passive confining pressure can effectively improve the dynamic ultimate strength of materials. Verification through numerical calculations has shown that the experimental data are consistent with the numerical calculation results, proving the effectiveness of this method (Ping et al., 2014; Jiao et al., 2021; Zhai et al., 2019; Li et al., 2009; Chen et al., 2011). This method is now widely used for dynamic mechanical property testing of rocks (Ping et al., 2014), coal (Jiao et al., 2021), concrete (Zhai et al., 2019; Li et al., 2009; Chen et al., 2011), soil (Tang et al., 2020; Zhu et al., 2020), sand (Chen H. et al., 2022; Song et al., 2009; Varley et al., 2020), explosives (Lan et al., 2011), and other materials under confining pressure conditions. For example, Shi et al. (Shi et al., 2000) used the SHPB passive confining pressure test method to study the dynamic mechanical response of cement mortar stone under quasi-one-dimensional strain. They analyzed and discussed the influence of the material properties and geometric dimensions of the confining pressure sleeve on the test results. Luo et al. (Luo et al., 2011) conducted a comparative study on the dynamic compression behavior of sand samples with different initial mass densities under rigid constraints. The research results show that the initial mass density of sand has a significant impact on its triaxial dynamic mechanical response. Ping et al. (Ping et al., 2014) used a 45# steel sleeve to circumferentially constrain coal mine rock materials, and used a variable cross-section Hopkinson bar to study the dynamic mechanical properties and deformation failure laws of the rock under passive confining pressure conditions. They found that under passive confining pressure conditions, the load-bearing capacity and resistance to deformation of rocks increased significantly. Experimental research data from various materials consistently demonstrate that this method can be utilized to study the dynamic mechanical properties of materials under lateral constraints.

Relevant scholars have also conducted extensive experimental research on the dynamic mechanical behavior of rocks at negative temperatures. Lin et al. (2021) studied the dynamic tensile mechanical properties of sandstone in the temperature range of −5°C to −30°C based on a split Hopkinson pressure bar experimental system. The study found that the dynamic tensile strength of sandstone increases first and then decreases with decreasing temperature. Li et al. (2018) conducted nuclear magnetic resonance and dynamic loading tests on rocks subjected to freeze-thaw cycles, studying the impact of freeze-thaw cycles on the pore structure and dynamic mechanical properties of rocks. They also analyzed the deterioration mechanism of rocks due to freeze-thaw cycles from the perspective of rock mesostructure. Ma et al. (2024) studied the dynamic mechanical behavior of rocks with defects using a drop hammer impact method, and analyzed the effect of freezing temperature on the strength of single-defect rocks. The study found that pore ice has a strengthening effect on rock strength within a certain temperature range, but below a certain temperature, pore ice can cause frost heaving damage to rocks. Su et al. (2023) studied the influence of freezing temperature on the dynamic tensile strength and crack propagation of sandstone through a combination of experiments and simulations. The study showed that the freezing temperature has a significant impact on the strain rate sensitivity and failure mode of sandstone.

Most of the above studies focus on exploring the dynamic mechanical behavior of rocks under lateral constraints or negative temperatures. However, considering the actual engineering construction conditions, the research on the mechanical response of weakly cemented rocks under the comprehensive action of multiple variables is clearly insufficient. This article focuses on the lateral constraint effect of shaft wall and other structures on rock layers, and uses an modified Hopkinson bar experimental system to carry out dynamic compression tests on frozen weakly cemented red sandstone under lateral constraints. The relationship between loading rate, temperature, constraint state and its dynamic mechanical characteristic parameters is analyzed. The research results have certain guiding significance for engineering design of frozen rock mass under dynamic loading.

TABLE 1 Mineral composition of weakly cemented red sandstone.

Rock name	Mineral content percentage (%)						
	Quartz	Plagioclase	Potassium feldspar	Calcite	Hard gypsum	Iron dolomite	Clay mineral
Weakly cemented red sandstone	53.4	28.0	12.3	4.1	0.6	0.4	A small amount

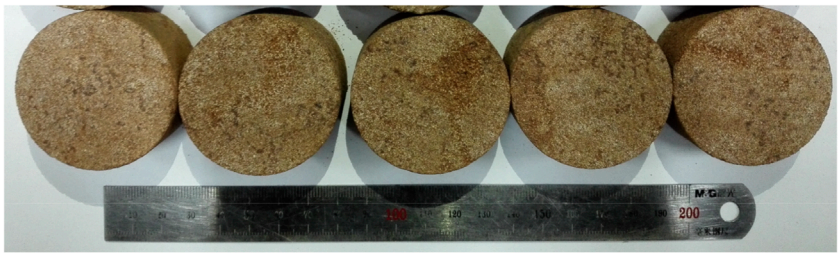

FIGURE 1
Weakly cemented red sandstone samples.

2 Experimental materials and equipment

The weak-cemented red sandstone studied is a typical sedimentary rock, with a dark red color and no obvious fissure development. The main components of the rock are quartz (53.4%), plagioclase (28.0%), potassium feldspar (12.3%), and other mineral components are detailed in Table 1. Select large blocks of weak-cemented red sandstone with good integrity and homogeneity, coring, cutting, and polishing to form cylindrical rock samples with a diameter of 50 mm and a height of 25 mm. The sample size and processing accuracy meet the test requirements (Dai et al., 2010). The processed rock samples are shown in Figure 1.

Based on the on-site freezing temperature, the test temperature range is set to −25°C–25°C. Prior to the test, a vacuum saturation device and a constant temperature freezing device are required to saturate and freeze the rock samples to obtain rocks at negative temperatures. Both saturation and freezing are set to last for 48 h. It is worth noting that during the freezing process, the water inside the rock will migrate and precipitate ice crystals on the rock surface. Therefore, after the water saturation is complete, it is necessary to apply Vaseline and plastic wrap to wrap the rock sample.

The SHPB experimental system integrated with a cold temperature module was used to conduct dynamic experiments on rocks at negative temperatures. The experimental system consists of the SHPB device and the cold temperature module, and it applies lateral constraints to the specimen through a metal sleeve. This experimental system is capable of testing the dynamic mechanical behavior of rock specimens under negative temperature and lateral constraint conditions, as shown in Figure 2. The experiment used cylindrical bars with a diameter of 50 mm as the striker and waveguide bars. The lengths of the striker, incident bar, and transmitted bar were 400 mm, 2,200 mm, and 1800 mm, respectively. Both the striker and waveguide bars were made of 7A04 aluminum, with an elastic modulus E_b of 70 GPa, a density ρ_b of 2,710 kg/m^3, and a yield strength σ_{Al} of 370 MPa. In the cold temperature module, the freezing tube connected to the liquid nitrogen device provides a negative temperature environment for the chamber, while using plexiglass as the front baffle of the chamber allows visualization of the loading process. By adjusting the pressure within the launch cavity, the speed of the striker is altered, thereby altering the loading rate of the specimen. The study investigated the temperature and strain rate effects on the dynamic mechanical response of frozen weakly cemented rock specimens under lateral constraint, analyzed the dynamic mechanical properties of weakly cemented rock specimens under lateral constraint, and studied the influence of lateral constraint on the dynamic compressive strength of rock specimens.

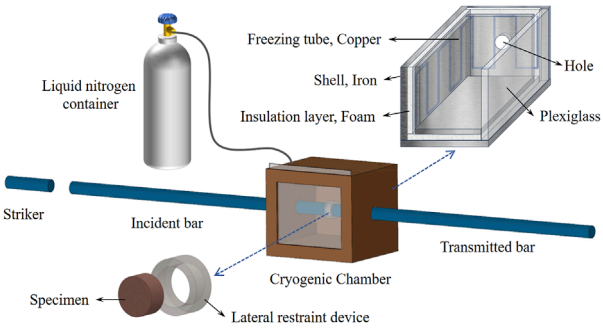

FIGURE 2
Schematic layout of the modified SHPB system integrated with the cold temperature sub-system.

3 Experimental principle

Based on the fundamental principles of the SHPB experimental technique, during the dynamic loading process, the strain and strain rate of the specimen can be determined by the displacement at both ends of the specimen, and the stress of the specimen can be determined by the force applied at both ends of the specimen. Furthermore, these parameters can be further determined by the incident, reflected, and transmitted waves at both ends of the specimen. Since the experiment uses a slender bar as the waveguide bar, satisfying the assumption of one-dimensional stress waves, there is no distortion in the propagation of elastic waves in the incident and transmitted bars (Wang, 2011). Therefore, the incident wave signal ε_{in} and the reflected wave signal ε_{re} can be acquired by the strain gauge attached to the middle of the incident bar, and the transmitted wave ε_{tr} signal can be acquired by the strain gauge attached to the middle of the transmitted bar. The stress σ_s, strain ε_s, and strain rate $\dot{\varepsilon}_s$ of the specimen can be calculated using Equation 1 (Yao et al., 2024).

$$\begin{cases} \sigma_s = \left(E_b A_b / 2A_s\right)\left[\varepsilon_{in}(t) + \varepsilon_{re}(t) + \varepsilon_{tr}(t)\right] \\ \varepsilon_s = \left(C_b / l_s\right)\int_0^{t_0}\left(\varepsilon_{in} - \varepsilon_{re} - \varepsilon_{tr}\right)dt \\ \dot{\varepsilon}_s = \left(C_b / l_s\right)\left(\varepsilon_{in} - \varepsilon_{re} - \varepsilon_{tr}\right) \end{cases} \tag{1}$$

In the formula, A_b and C_b represent the cross-sectional area and longitudinal wave velocity of the bar, respectively, while A_s and l_s represent the cross-sectional area and length of the specimen, respectively.

The experiment uses an aluminum sleeve to provide lateral constraints for the rock sample, as shown in Figure 3. To ensure the close contact between the rock sample and the aluminum sleeve, and to ensure the effective transmission of stress, this article uses the special pure wear-resistant yellow grease produced by Beijing Huahang Feitian Lubricant Sales Company as a coupling agent. This type of grease is relatively viscous and has strong adhesion, making it difficult to spill when under load. Its incompressibility also ensures effective conduction of stress. Therefore, this type of grease is used in the experiment to fill the small gaps between the sample and the aluminum sleeve, ensuring close contact between the rock and the sleeve. The aluminum sleeve used in the experiment is a thick-walled sleeve, and the diameter change of the sleeve is measured after each impact to ensure that the sleeve is always in an elastic state, simulating the elastic constraint effect of the surrounding infinite medium on the rock mass when it is disturbed. The pressure p_1 on the inner wall of the sleeve and the radial displacement U_r of the inner wall can be calculated by Equation 2. When the inner wall of the sleeve is closely fitted to the sample and satisfies the equilibrium conditions, the radial stress σ_r, hoop stress σ_θ, radial strain ε_r, and hoop strain ε_θ of the sample can be calculated by Equation 3 (Tang et al., 2020).

$$\begin{cases} p_1 = -\dfrac{R_2^2 - R_1^2}{2R_1^2} E_j \varepsilon_j \\ U_r = -\dfrac{R_1 \varepsilon_j}{2}\left[\left(1 - \upsilon_j\right) + \left(1 + \upsilon_j\right)\dfrac{R_2^2}{R_1^2}\right] \end{cases} \tag{2}$$

FIGURE 3
Aluminum sleeve used in the test.

$$\begin{cases} \sigma_r = \sigma_\theta = p_1 = -\dfrac{R_2^2 - R_1^2}{2R_1^2} E_j \varepsilon_j \\ \varepsilon_r = \varepsilon_\theta = \dfrac{\varepsilon_j}{2}\left[\left(1 - \upsilon_j\right) + \left(1 + \upsilon_j\right)\dfrac{R_2^2}{R_1^2}\right] \end{cases} \tag{3}$$

In the formula, ε_j represents the strain of the outer ring of the aluminum sleeve, which is collected through strain gauges. R_1 is the inner radius of the aluminum sleeve, which is 25.2 mm R_2 is the outer radius of the aluminum sleeve, which is 29.2 mm. The elastic modulus of the aluminum sleeve is E_j = 70 GPa, and the Poisson's ratio is υ_j = 0.33.

4 Experimental results

Figure 4A–E shows the relationship between dynamic compressive stress and strain of frozen water-saturated weakly cemented rock samples under lateral constraints. As can be seen from Figure 4, temperature and strain rate have a significant influence on the dynamic compressive properties of weakly cemented rock samples under the same coordinate scale. Meanwhile, combined with previous research results (Fang et al., 2023), it is not difficult to find that compared with uniaxial compression, the strength and critical strain of rock under lateral constraint are greatly improved. Figure 4F shows a typical curve shape. It can be seen from the figure that the deformation process of the rock samples goes through three stages: a longer compaction stage (Section 1), a rapid stress increase stage

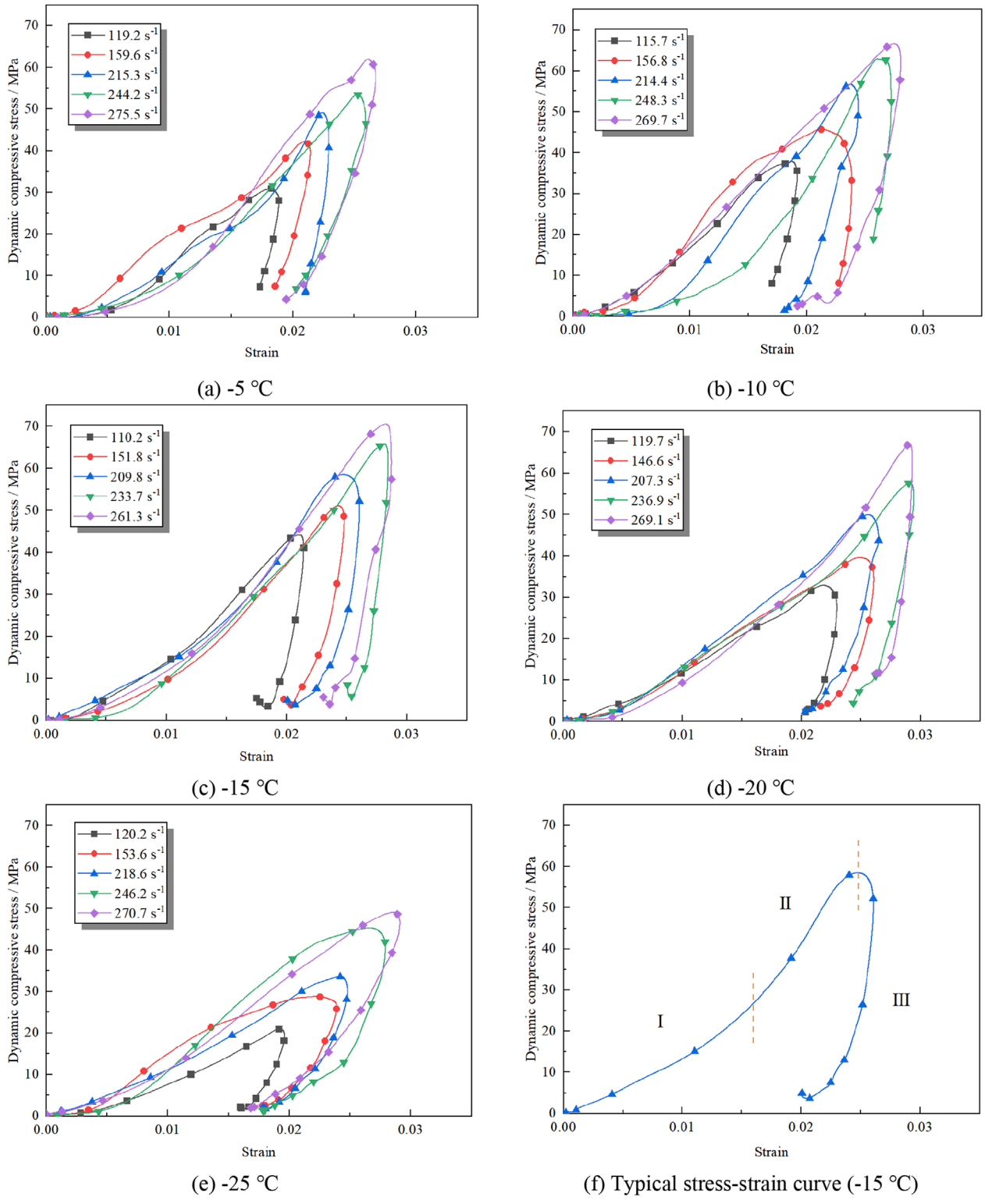

FIGURE 4
Dynamic compressive stress-strain curve of frozen water-saturated weakly cemented rock samples under lateral constraints.

(Section 2), and an unloading stage (Section 3). Compared with uniaxial compression, it has a longer compaction stage and obvious rebound characteristics.

The axial stress σ_Z of the specimen can be determined by Equation (1), where $\sigma_Z = \sigma_s$. Figure 5 shows the typical curve of the relationship between confining stress and axial stress. As can

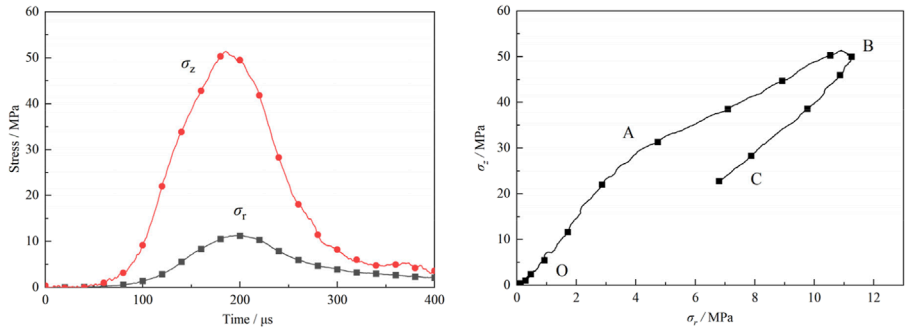

(a) Axial and confining pressure stress history curve

(b) Curve of axial stress varying with confining pressure stress

FIGURE 5
Relationship between axial stress and confining pressure stress.

be seen from Figure 5A, the axial stress and confining stress change simultaneously, reaching their peak values at around 200 μs. This is because the confining stress is generated by the axial compressive stress. The greater the axial compressive stress, the greater the deformation of the specimen, and the greater the force on the lateral aluminum sleeve, resulting in stronger reverse constraint. Therefore, the stress-time curves of the two are synchronized. Figure 5B shows the relationship between axial stress and confining stress. It can be observed that the relationship can be divided into three stages. Initially, the axial stress and confining stress are linearly related, with the magnitude of the confining stress increasing as the axial stress increases (OA segment). As the axial stress further increases, the increase in confining stress decreases, and a clear turning point appears at point A. After reaching point B, the loading is completed and unloading begins, with the confining stress falling synchronously as the axial stress decreases. The mechanical characteristic parameters of the dynamic compressive stress-strain curve under lateral constraint are extracted and shown in Table 2.

5 Combined effects of multiple variables

5.1 Strain rate effect of dynamic compressive strength

From Table 2, it can be observed that at the same temperature, the strength of the sample is closely related to the strain rate. Taking −15°C as an example, the dynamic compressive strength is 44.1 MPa at a strain rate of 110.2 s^{-1}. As the strain rate increases to 151.8 s^{-1}, the strength increases by 16.1%–51.3 MPa. At strain rates of 209.8 s^{-1}, 233.7 s^{-1}, and 261.3 s^{-1}, the strengths are 58.5 MPa, 65.3 MPa, and 70.6 MPa, respectively. Compared to the strength at 110.2 s^{-1}, the increase rates are 32.9%, 48.1%, and 60.1%, respectively. It can be found that as the strain rate increases, the strength gradually increases. When there is lateral constraint, the dynamic compressive strength of rock samples at various temperatures is nonlinearly positively correlated with the strain rate. The exponential function is used to fit the relationship between dynamic compressive strength and strain rate under lateral restraint, and the fitting results are shown in Figure 6 and Equation 4.

$$\begin{cases} T = 25°C, DCS_L = 9.68\exp(0.0078\dot{\varepsilon}), R^2 = 0.9992 \\ T = -5°C, DCS_L = 21.36\exp(0.0039\dot{\varepsilon}), R^2 = 0.9730 \\ T = -10°C, DCS_L = 25.67\exp(0.0036\dot{\varepsilon}), R^2 = 0.9941 \\ T = -15°C, DCS_L = 31.64\exp(0.0031\dot{\varepsilon}), R^2 = 0.9911 \\ T = -20°C, DCS_L = 20.14\exp(0.0044\dot{\varepsilon}), R^2 = 0.9961 \\ T = -25°C, DCS_L = 11.41\exp(0.0054\dot{\varepsilon}), R^2 = 0.9526 \end{cases} \quad (4)$$

5.2 Temperature effect of dynamic compressive strength

To illustrate the variation of dynamic compressive strength of water-saturated weakly cemented red sandstone under lateral confinement with temperature, Figure 7 shows the curves of dynamic compressive strength *versus* temperature at average strain rates of 114.9 ± 10.6 s^{-1}, 153.9 ± 7.3 s^{-1}, 211.2 ± 9.6 s^{-1}, 239.9 ± 9.8 s^{-1}, and 268.3 ± 7.0 s^{-1}. As the temperature decreases from 25°C to −25°C, the dynamic compressive strength of water-saturated weakly cemented red sandstone at each strain rate shows a trend of first increasing and then decreasing. Within the range of 25°C to −15°C, the strength increases with decreasing temperature, while within the range of −15°C to −25°C, the strength decreases with decreasing temperature. Taking the average strain rate of (211.2 ± 9.6 s^{-1}) as an example, the strength is 45.9 MPa at 25°C. After entering the negative temperature range, the strength begins to increase, reaching 50.1 MPa and 56.7 MPa at −5°C and −10°C, respectively. The maximum strength is reached at −15°C, which is 58.5 MPa. Subsequently, the strength begins to decrease, reaching 50.1 MPa and 33.5 MPa at −20°C and −25°C, respectively. Compared to −15°C, the decreases are 14.4% and 42.7%, respectively. The reason for the above phenomenon is that the low-temperature

TABLE 2 Dynamic mechanical parameters of frozen water-saturated weakly cemented rock samples under lateral constraint.

Sample number	Strain rate $\dot{\varepsilon}$ /s^{-1}	DCS_L/MPa	Sample number	Strain rate $\dot{\varepsilon}$ /s^{-1}	DCS_L/MPa
LSDC-25–1	104.3	21.2	LSDC--15–1	110.2	44.1
LSDC-25–2	154.7	33.1	LSDC--15–2	151.8	51.3
LSDC-25–3	201.6	45.9	LSDC--15–3	209.8	58.5
LSDC-25–4	230.1	57.4	LSDC--15–4	233.7	65.3
LSDC-25–5	263.7	75	LSDC--15–5	261.3	70.6
LSDC--5–1	119.2	31.6	LSDC--20–1	119.7	33.3
LSDC--5–2	159.6	42.3	LSDC--20–2	146.6	39.9
LSDC--5–3	215.3	50.1	LSDC--20–3	207.3	50.1
LSDC--5–4	244.2	53.8	LSDC--20–4	236.9	57.6
LSDC--5–5	275.5	62.3	LSDC--20–5	269.1	66.5
LSDC--10–1	115.7	38.3	LSDC--25–1	120.2	20.9
LSDC--10–2	156.8	44.6	LSDC--25–2	153.6	28.7
LSDC--10–3	214.4	56.7	LSDC--25–3	218.6	33.5
LSDC--10–4	248.3	62.5	LSDC--25–4	246.2	45.4
LSDC--10–5	269.7	66.4	LSDC--25–5	270.7	49.1

Note: LSDC, stands for "Lateral restraint, Saturated, Dynamic, Compression", and the number after the letter is the temperature, for example, −5 indicates a freezing temperature of −5°C. The last number is the serial number of the sample. DCS_L, stands for "Dynamic Compressive Strength, Lateral restraint".

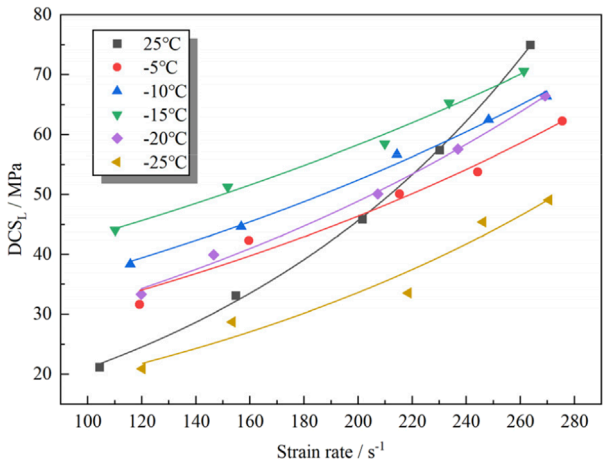

FIGURE 6
Relationship between dynamic compressive strength and strain rate of frozen weakly cemented rock samples under lateral constraints.

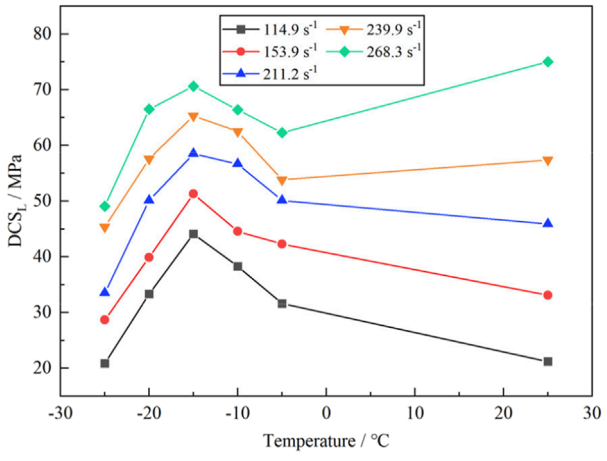

FIGURE 7
Relationship between DCS_L and temperature.

environment has both positive and negative effects on rocks (Weng et al., 2019; Weng et al., 2020). The strength characteristics of rocks are closely related to their internal ice water phase transition at low temperatures. For the rocks studied in this article, the transition point between the two occurs at −15°C, which leads to the occurrence of the above phenomenon.

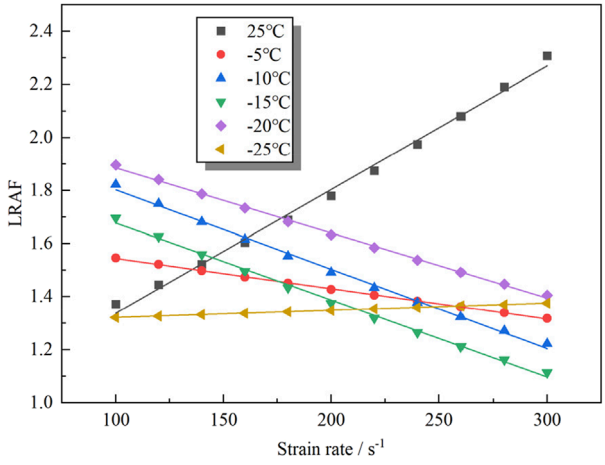

FIGURE 8
Relationship between LRAF and strain rate.

5.3 Influence of lateral constraint on the dynamic compression characteristics

To visually demonstrate the influence of lateral restraint on dynamic compressive strength, the Lateral Restraint Affecting Factor (LRAF) is introduced. LRAF is the ratio of the strength value under lateral restraint to the uniaxial dynamic strength. Based on previous research results (Fang et al., 2023), the rock strength under uniaxial and lateral restraint conditions is compared. Figure 8 shows the relationship between LRAF and strain rate. It can be found from the figure that the LRAF values at various temperatures are all greater than 1, indicating that the effect of lateral restraint on strength improvement is significant. Compared with the trend of LRAF increasing with strain rate at room temperature, LRAF decreases with strain rate at all temperatures except for a slight increase at −25°C. The relationship between LRAF and strain rate at each temperature was fitted using the linear equation LRAF = C + D*(strain rate), and the fitting parameters are shown in Table 3. From the fitted slope, it is found that LRAF has a negative correlation with strain rate in the range of −5°C to −20°C, and LRAF has a positive correlation with strain rate at −25°C, but the increase rate is slow.

Figure 9 is a comparison diagram of dynamic compressive strength under uniaxial and lateral constraints. It can be found from the diagram that the compressive strength under lateral constraints is higher than that under uniaxial compression, showing a significant lateral constraint strengthening effect, as indicated by the blue arrow in the diagram. The yellow arrow in the diagram reflect the strain rate strengthening effect of weakly cemented rock samples. Under various working conditions, the dynamic strength of rock samples increases with the increase of strain rate. The temperature effect is shown by the red arrow in the diagram. As the freezing temperature decreases, the dynamic compressive strength under both uniaxial and lateral constraints shows a trend of first increasing and then decreasing, with the strength turning point occurring at −15°C.

5.4 Macroscopic failure morphology of rocks

Under similar strain rates and lateral constraints, the failure morphology of frozen weakly cemented rocks after impact loading is shown in Figure 10. From Figure 10, it can be found that in the temperature range from −5°C to −20°C, the degree of rock failure is relatively low, and shear failure is the main mode of failure. At −5°C, −10°C, and −15°C, the rock remains almost intact, with only local shear failure and a small amount of spalling at the edges, and almost no macroscopic cracks on the surface. However, as the temperature continues to decrease, the degree of rock failure gradually increases. At −20°C, the shear failure surface increases and basically penetrates the entire rock sample. When the temperature drops to −25°C, the main mode of rock failure changes from shear failure to tensile failure. At this temperature, the rock exhibits crushing failure, with the rock sample mainly splitting into several large blocks, accompanied by small blocks formed by local shear. However, from its stress-strain curve, there is still a rebound phenomenon, which may be due to the fact that the rock is constrained in a limited space and can still bear the load. Overall, the degree of rock fragmentation at negative temperatures decreases first and then increases with decreasing temperature. Therefore, under the influence of negative temperatures, the degree of rock fragmentation and strength characteristics maintain a good consistency.

6 Conclusion

This article uses an modified SHPB experimental system to conduct dynamic compression tests on water-saturated weakly cemented red sandstone samples under negative temperature and lateral constraints at different impact velocities. The dynamic mechanical properties of weakly cemented rocks under the combined effects of multiple variables were studied, and the effects of negative temperature gradient, loading rate, and constraint conditions on the dynamic mechanical response of water-saturated weakly cemented red sandstone were analyzed. The main conclusions are as follows.

(1) The lateral passive confining pressure and axial stress change synchronously, reaching their peak values simultaneously at 200 μs. The interaction process between axial stress and hoop stress can be divided into three stages: rapid increase, slow increase, and unloading rebound stage.
(2) The dynamic mechanical parameters of the rock show a significant strain rate effect, with both peak strain and dynamic compressive strength increasing with the increase of strain rate, and the dynamic compressive strength is exponentially related to the strain rate.
(3) Under the combined action of lateral constraints and dynamic loads, the deformation of frozen rocks goes through three stages: compaction stage, rapid stress increase stage, and unloading stage. Compared with uniaxial compression, the dynamic stress-strain curve of frozen rock under lateral constraint shows obvious compaction and rebound characteristics, and both strength and critical strain have been significantly improved.

TABLE 3 Function parameters for linear fit between LRAF and strain rate.

Temperature	25°C	−5°C	−10°C	−15°C	−20°C	−25°C
C	0.87	1.66	2.10	1.97	2.13	1.29
D	0.0047	−0.0011	−0.0030	−0.0029	−0.0025	0.0003
R^2	0.99477	0.9995	0.99689	0.99658	0.99825	0.99997

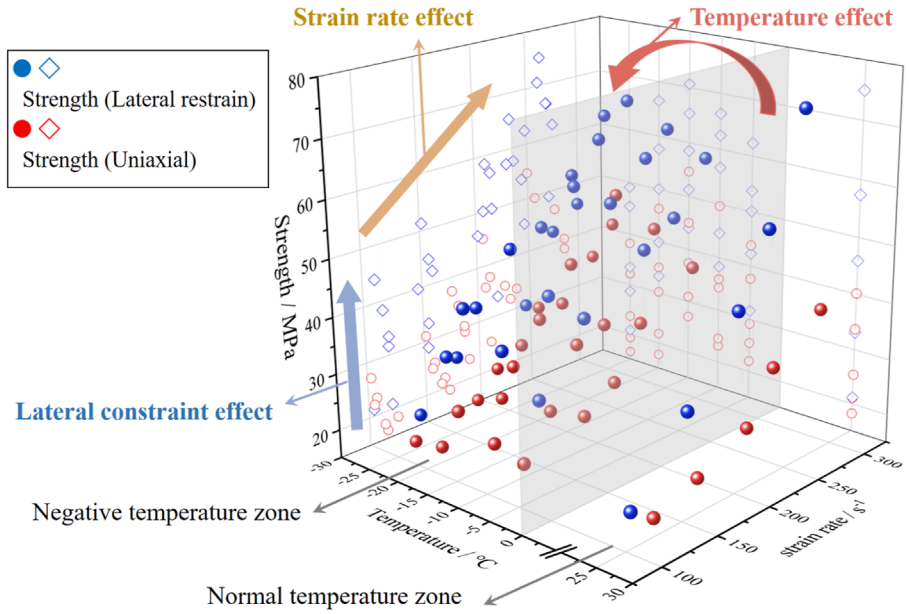

FIGURE 9
Comprehensive comparison diagram of rock compressive strength under uniaxial and lateral constraints.

FIGURE 10
Macroscopic fragmentation morphology of frozen weakly cemented rock under lateral confinement (269.5 ± 17.9 s^{-1}).

(4) The lateral confinement effect significantly enhances the dynamic compressive strength of rocks, and the influence factor of lateral confinement is greater than one at all temperatures. There is a negative linear correlation between LRAF and strain rate within the range of −5°C to −20°C, and a positive linear correlation between LRAF and strain rate at −25°C.

(5) Within the temperature range of −5°C to −25°C, as the temperature decreases, the dynamic compressive strength of frozen rocks first increases and then decreases, and the degree of fragmentation first decreases and then increases. The main form of failure transitions from shear failure to tensile failure. And −15°C is the transition temperature for strength, fragmentation degree, and failure mode.

Data availability statement

The original contributions presented in the study are included in the article/supplementary material, further inquiries can be directed to the corresponding author.

Author contributions

WL: Funding acquisition, Project administration, Supervision, Validation, Writing–original draft, Writing–review and editing. SF: Data curation, Formal Analysis, Investigation, Writing–original draft. YZ: Conceptualization, Methodology, Resources, Writing–original draft. GL: Software, Visualization, Writing–original draft.

Funding

The author(s) declare that financial support was received for the research, authorship, and/or publication of this article. This research was supported by: 1) National Natural Science Foundation of China (Grant No. 52304116), 2) Open Research Grant of Joint National-Local Engineering Research Centre for Safe and Precise Coal Mining (Grant No. EC2025016), 3) Scientific Research Foundation for High-level Talents of Anhui University of Science and Technology (Grant No. 2021yjrc25).

Conflict of interest

Author SF was employed by China Jingye Engineering Co., Ltd. Author GL was employed by Shandong Succeed Mining Safety Engineering Co.

The remaining authors declare that the research was conducted in the absence of any commercial or financial relationships that could be construed as a potential conflict of interest.

Publisher's note

References

Bai, Y., Shan, R., Ju, Y., Wu, Y., Sun, P., and Wang, Z. (2020). Study on the mechanical properties and damage constitutive model of frozen weakly cemented red sandstone. *Cold Regions Sci. Technol.* 171, 102980. doi:10.1016/j.coldregions.2019.102980

Bi, Z., Liu, J., Zhao, F., Wang, Y., and Zhen, M. (2024). Research on dynamic constitutive model of steel fiber reinforced concrete with different steel fiber content and matrix strength. *Constr. Build. Mater.* 433, 136671. doi:10.1016/j.conbuildmat.2024.136671

Bragov, A. M., Lomunov, A. K., Sergeichev, I. V., Tsembelis, K., and Proud, W. (2008). Determination of physicomechanical properties of soft soils from medium to high strain rates. *Int. J. Impact Eng.* 35 (9), 967–976. doi:10.1016/j.ijimpeng.2007.07.004

Cai, H., Liu, Z., Li, S., and Zheng, T. (2019). Improved analytical prediction of ground frost heave during tunnel construction using artificial ground freezing technique. *Tunn. Undergr. Space Technol.* 92, 103050. doi:10.1016/j.tust.2019.103050

Chen, H., Zhang, C., Wei, J., Li, M., and Wang, Y. (2022b). A modified method for estimating the stress state of granular materials in the passive confined pressure SHPB tests. *Int. J. Impact Eng.* 160, 104063. doi:10.1016/j.ijimpeng.2021.104063

Chen, J. Y., Zhang, Z. X., Dong, H. W., and Zhu, J. (2011). Experimental study on dynamic damage evolution of concrete under multi-axial stresses. *Eng. Fail. Anal.* 18 (7), 1784–1790. doi:10.1016/j.engfailanal.2011.04.006

Chen, S., Zhang, H., Wang, L., Yuan, C., Meng, X., Yang, G., et al. (2022a). Experimental study on the impact disturbance damage of weakly cemented rock based on fractal characteristics and energy dissipation regulation. *Theor. Appl. Fract. Mech.* 122, 103665. doi:10.1016/j.tafmec.2022.103665

Dai, F., Huang, S., Xia, K., and Tan, Z. (2010). Some fundamental issues in dynamic compression and tension tests of rocks using split Hopkinson pressure bar. *Rock Mech. Rock Eng.* 43 (6), 657–666. doi:10.1007/s00603-010-0091-8

Fang, S., Yang, Y., Zhao, Y., Chen, J., and Li, W. (2023). Dynamic mechanical properties and energy dissipation of frozen weakly cemented red sandstone under high strain rate loading. *Bull. Eng. Geol. Environ.* 82 (11), 418. doi:10.1007/s10064-023-03436-5

Jiao, Z. H., Mu, C. M., Wang, L., Cui, Z. L., Yuan, Q. P., Zou, P., et al. (2021). Tests for dynamic mechanical properties of coal impact compression under passive confining pressure. *J. Vib. Shock* 40 (21), 185–193. doi:10.13465/j.cnki.jvs.2021.21.025

Lan, L. G., Wen, M. P., Li, M., Pang, H. Y., and Jing, S. M. (2011). Impact mechanical properties of PBX in passive confined pressure. *Chin. J. Explos. Propellants* 4, 41–44.

Li, J., Kaunda, R. B., and Zhou, K. (2018). Experimental investigations on the effects of ambient freeze-thaw cycling on dynamic properties and rock pore structure deterioration of sandstone. *Cold Regions Sci. Technol.* 154, 133–141. doi:10.1016/j.coldregions.2018.06.015

Li, X. L., Liu, D. S., Feng, M. D., Li, S. L., and Yan, Z. G. (2009). Dynamic mechanical properties of concrete materials subjected to passive confining pressure produced by a steel sleeve. *Explos. Shock Waves* 5 (2).

Li, Y. Y., Zhang, S. C., Yang, Y. M., Chen, H. R., Li, Z. K., and Ma, Q. (2022). Study on the water bursting law and spatial distribution of fractures of mining overlying strata in weakly cemented strata in West China. *Geomechanics Eng.* 28 (6), 613–624. doi:10.12989/gae.2022.28.6.613

Lin, G., Li, M., Chen, Y., Zhang, J., Jiskani, I. M., Doan, D. V., et al. (2021). Dynamic tensile mechanical properties and fracture characteristics of water-saturated sandstone under the freezing effect. *Int. J. Geomechanics* 21 (5), 04021044. doi:10.1061/(asce)gm.1943-5622.0001999

Liu, S., Yang, G., Liu, H., Dong, X., and Shen, Y. (2023). Study on the acoustic emission characteristics and failure precursors of water-rich frozen sandstone under different lateral unloading rates. *Water* 15 (12), 2297. doi:10.3390/w15122297

Luo, H., Cooper, W. L., and Lu, H. (2014). Effects of particle size and moisture on the compressive behavior of dense Eglin sand under confinement at high strain rates. *Int. J. Impact Eng.* 65, 40–55. doi:10.1016/j.ijimpeng.2013.11.001

Luo, H., Lu, H., Cooper, W. L., and Komanduri, R. (2011). Effect of mass density on the compressive behavior of dry sand under confinement at high strain rates. *Exp. Mech.* 51, 1499–1510. doi:10.1007/s11340-011-9475-2

Ma, K., Ren, F., Wang, H., Li, L., and Wu, D. (2024). Dynamic mechanical responses and freezing strengthening mechanism of frozen sandstone with single flaw: insights from drop weight tests and numerical simulation. *Rock Mech. Rock Eng.* 57 (2), 1263–1285. doi:10.1007/s00603-023-03614-7

Ping, Q., Ma, Q. Y., Lu, X. Y., and Yuan, P. (2014). Impact compression test of rock material under passive confining pressure conditions. *Chin. J. Vib. Shock* 33 (2), 55–59.

Shan, R., Bai, Y., Ju, Y., Han, T. y., Dou, H. y., and Li, Z. l. (2021). Study on the triaxial unloading creep mechanical properties and damage constitutive model of red sandstone containing a single ice-filled flaw. *Rock Mech. Rock Eng.* 54, 833–855. doi:10.1007/s00603-020-02274-1

Shi, S. Q., Chen, J. Y., Li, D. H., and Wang, L. L. (2000). A study on the dynamic mechanical behavior of cement mortar under quasi-one dimensional strain state. *Explos. Shock Waves* 20 (4), 326–332.

Song, B., Chen, W., and Luk, V. (2009). Impact compressive response of dry sand. *Mech. Mater.* 41 (6), 777–785. doi:10.1016/j.mechmat.2009.01.003

Su, H., Zhu, Z., and Wang, L. (2023). Experimental and numerical analysis of dynamic splitting mechanical properties and crack propagation for frozen sandstone. *Int. J. Rock Mech. Min. Sci.* 163, 105325. doi:10.1016/j.ijrmms.2022.105325

Tang, W. R., Zhu, Z. W., Fu, T. T., Zhou, Z. W., and Shangguan, Z. H. (2020). Dynamic experiment and numerical simulation of frozen soil under confining pressure. *Acta Mech. Sin.* 36, 1302–1318. doi:10.1007/s10409-020-00999-4

Varley, L., Rutherford, M. E., Zhang, L., and Pellegrino, A. (2020). The mechanical response of wet volcanic sand to impact loading, effects of water content and initial compaction. *J. Dyn. Behav. Mater.* 6, 358–372. doi:10.1007/s40870-020-00257-5

Wang, L. (2011). *Foundations of stress waves*. Elsevier.

Wang, Y. S., and Yang, R. (2022). Monitoring and analysis of the stress and deformation of shaft lining and the influence of freezing tube fracture in deep topsoil. *Cold Regions Sci. Technol.* 193, 103420. doi:10.1016/j.coldregions.2021.103420

Weng, L., Wu, Z., and Liu, Q. (2020). Dynamic mechanical properties of dry and water-saturated siltstones under sub-zero temperatures. *Rock Mech. Rock Eng.* 53, 4381–4401. doi:10.1007/s00603-019-02039-5

Weng, L., Wu, Z., Liu, Q., and Wang, Z. (2019). Energy dissipation and dynamic fragmentation of dry and water-saturated siltstones under sub-zero temperatures. *Eng. Fract. Mech.* 220, 106659. doi:10.1016/j.engfracmech.2019.106659

Xu, C., Yang, Y., Hou, S., and Zhang, H. (2024). Investigations on the freezing characteristic and flexural mechanical properties of frozen loess. *Cold Regions Sci. Technol.* 217, 104060. doi:10.1016/j.coldregions.2023.104060

Yao, W., Li, X., Xu, Y., and Wu, B. (2024). Preliminary analysis of the end friction effect on dynamic compressive strength of rocks. *Rock Mech. Rock Eng.* 57, 8899–8910. doi:10.1007/s00603-024-03950-2

Zhai, Y., Li, Y., Li, Y., Zhang, Y., Meng, F., and Lu, M. (2019). Impact compression test and numerical simulation analysis of concrete after thermal treatment in complex stress state. *Materials* 12 (12), 1938. doi:10.3390/ma12121938

Zhang, W., Zhang, B., and Zhao, T. (2023). Study on the law of failure acoustic–thermal signal of weakly cemented fractured rock with different dip angles. *Rock Mech. Rock Eng.* 56 (6), 4557–4568. doi:10.1007/s00603-023-03296-1

Zheng, Z. T., Xu, Y., Dong, J. H., Zong, Q., and Wang, L. P. (2015). Hard rock deep hole cutting blasting technology in vertical shaft freezing bedrock section construction. *J. Vibroengineering* 17 (3), 1105–1119.

Zhu, Z., Cao, C., and Fu, T. (2020). SHPB test analysis and a constitutive model for frozen soil under multiaxial loading. *Int. J. Damage Mech.* 29 (4), 626–645. doi:10.1177/1056789519867471